Biomedical Signal Processing and Control 18 (2015) 195–203

Contents lists available at ScienceDirect

Biomedical Signal Processing and Control

journal homepage: www.elsevier.com/locate/bspc

Quantitative analysis of live lymphocytes morphology and intracellular motion in microscopic images

Yali Huang [a,b], Zhiwen Liu [a,*], Yonggang Shi [a]

[a] School of Information and Electronics, Beijing Institute of Technology, Beijing, China
[b] College of Electronics and Information Engineering, Hebei University, Baoding, China

ARTICLE INFO

Article history:
Received 14 June 2014
Received in revised form 9 December 2014
Accepted 15 January 2015
Available online 6 February 2015

Keywords:
Lymphocyte shape analysis
Lymphocyte deformation analysis
Intracellular motion analysis
Optical flow

ABSTRACT

Cellular morphology and motility analysis is a key issue for abnormality identification and classification in the research of relevant biological processes. Quantitative measures are beneficial to clinicians in making their final diagnosis. This article presents a new method for measurement of live lymphocyte morphology and intracellular motion (motility) in microscopic images acquired from peripheral blood of mice post skin transplantation. Our new method explores shape, deformation and intracellular motion features of live lymphocytes. Especially, a novel way of exploiting intracellular motion information based on optical flow method is proposed. On the basis of statistical tests, optimal morphological and motility features are chosen to form a feature vector that characterizes the dynamic behavior of the lymphocytes (including shape, deformation and intercellular motion). In order to evaluate the proposed scheme, the above feature vector is used as input to a probabilistic neural network (PNN) which then classifies the dynamic behavior of lymphocytes in a set of cell image sequences into normal and abnormal categories. Comparative experiments are conducted to validate the proposed scheme, and the results revealed that joint features of shape, deformation and intracellular motion achieve the best performance in expressing the dynamic behavior of lymphocytes, compared with Fourier descriptor and Zernike moment methods.

1. Introduction

Measurement of live cells morphology and motility in microscopic images is essential to understanding and treating some biological processes, such as the development of an organism, wound healing, cancer metastasis, drug test, inflammation research and immune response [1–7]. Computer-assisted cell image analysis has become a powerful analytical tool for turning qualitative data into quantitative values [8–13]. As we know, lymphocytes are involved in immune response. Clinicians observed that lymphocytes are highly deformable objects: cell deformation and protrusion are more active when the graft rejection occurs, compared with the case of no graft rejection occurring. Currently, needle biopsy, the golden standard of pathology method to diagnose rejection, is far from satisfactory because it is invasive, time-consuming, trial-limited, and dependent on the puncture location [14]. The analysis of lymphocytes dynamic behavior to reveal the relationships between the immune status of the organism and activity of immune cells via microscopic images is meaningful for the assisted diagnosis of graft rejection. In this article, we focus on analyzing the dynamic behavior of the single lymphocyte in different situations, normal and abnormal (graft rejection), and then classify them based on quantitative assessment of lymphocytes' shape, deformation and intracellular motion.

In the past four decades, many applications of cell image analysis have been developed, such as the classification of white blood cells [15], cell segmentation and tracking [1,4,6,7,16–21], and the quantitative characterization of cells dynamic behavior [5,8,22–28]. Some shape parameters (center, area, perimeter, circularity, and minimum rectangle) were extracted, and the rate of the NIH-3T3 cell movement was calculated by measuring the displacement of the whole cell in [22]. The Weijer group introduced a gradient method for quantitative analysis of cell movement [23]. The velocity of the leukocyte was computed from a tangent direction at each point of the trace in [24]. Quantitative analysis of dynamic behavior (deformation and migration) of cells was presented in [5,25], in which motion and deformation parameters were extracted from parametric estimation of the affine-motion model. Theriot et al. studied on the mechanism of shape determination in motile cells,

* Corresponding author at: School of Information and Electronics, Beijing Institute of Technology, Beijing 100081, China. Tel.: +86 1068911432.
E-mail address: zwliu@bit.edu.cn (Z. Liu).

http://dx.doi.org/10.1016/j.bspc.2015.01.003
1746-8094/

and further predicted the cell's speed from its aspect ratio [26]. The method for local and global measures of shape dynamics was proposed in [27], and the cell motion speed was computed from the magnitude of the displacement of the boundary point. Our earlier work has presented a geometric method for modeling dynamic features of cells in image sequences, which emphasized on cell deformation analysis without considering intracellular movement [28].

In previous work on cell image analysis, there are two worth noting issues: first, in the analysis of cell motion, the cell speed was usually calculated via the displacement of the centroid of the cell [22], by the tangent direction of the motion trail of the cell [24], through the cell deformation [26], or via the affine-motion model [5,25]. All these methods dealt with the movement of the whole cell. Little attention has been paid to the intracellular motion [23]. Secondly, these works either dealt with shape and deformation analysis [8] or dealt with cell motion analysis [23,24]. However, few have combined these three aspects [22]. Quantitative methods for cell shape analysis mentioned in the article [8] do not provide information about the dynamic cellular activity.

In this article, in order to quantitatively assess the dynamic behavior of the lymphocyte, we computed the intracellular motion field directly using optical flow techniques based on the brightness constant model (BCM) [29], and further extracted intracellular motion feature from it. Especially we quantitatively analyzed the dynamic cellular activity from three aspects: shape, deformation and intracellular motion, and then combined three aspects of features to classify lymphocyte dynamic behavior into normal and abnormal categories. This article is an extended version of our preliminary work presented in the conference article [30].

The rest of the article is organized as follows. Materials and methods are introduced in Section 2. Experiments and results are presented in Section 3, and the discussion in Section 4. Finally, the conclusion is in Section 5.

2. Materials and methods

2.1. Materials

The cell image sequences were acquired by optical phase contrast microscope at a magnification of 160,00× from the peripheral blood samples of clean healthy mice 7 days after the skin transplantation. The mice in our experiments are 6–8 weeks and 20–22 g. Experiments ensure that there is only one object-lymphocyte in each frame image. That is to say we only observe one lymphocyte in each image sequence. The animal experiments were conducted by the trained staff in Beijing You'an Hospital, which is affiliated to the Capital Medical University. And the hospital is a Grade-III Class-A hospital of the Ministry of Health in China. All the disposals are in accordance with the guideline of animal ethics. Two kinds of experiments were conducted. The first experiment was implemented through autologous transplant. Healthy Balb/C male mice were used as both hosts and donors, which is called self-skin transplantation group (the SST group). The second experiment was implemented through allogenic transplantation, in which healthy Balb/C male mice were used as hosts while healthy C57BL/6 male mice were used as donors. We called it allogenic skin transplantation group (the AST group). The shape of the lymphocytes is stable in the SST group, and the deformation and intracellular motion are slight. There is no acute rejection in this case, and this is a normal group. The lymphocytes are more active in the AST group, and the deformation and intracellular motion are intense. There is acute rejection in this case, and it is an abnormal group.

2.2. Segmentation and tracking of the lymphocyte

Segmentation and tracking of cell boundaries in phase contrast microscopic images are challenging due to non-uniform edge intensities and the phase halos. Active contour models (snakes), pulling the initial contour to the desired boundaries with various kinds of external force, have shown prominent advantages in object segmentation and tracking. However, the current external-force-inspired snakes suffer from initialization sensitivity, and are weak at handling low-contrast edges. We propose a new feature map instead of the traditional edge map to generate external force field for snakes evolution, and apply it to cell segmentation and tracking in this study. The new feature map can combine the region information of the object, extracted by morphology gray-scale reconstruction (MGR), and the edge information, extracted by the Laplacian of Gaussian (Log) filter, which is called MGRL-feature map and defined as follows:

$$f_{\mathrm{MGRL}}(x,y) = F_l[\nabla^2(G_\sigma(x,y) \times \rho_{I(x,y)}(J(x,y)))] \tag{1}$$

where $F_1(\cdot)$ is a low pass filter; $\nabla^2(\cdot)$ is the Laplacian operator; $G_\sigma(x, y) + \rho_{I(x,y)}(J(x, y))$ is the convolution of the Gaussian function $G_\sigma(x, y)$ and $\rho_{I(x,y)}(J(x, y))$. $\rho_{I(x,y)}(J(x, y))$ denotes the MGR of the $I(x, y)$ from the $J(x, y)$. $I(x, y)$ is the region of interest (ROI). The details of the MGR process can be found in [31]. The improved external force field based on MGRL-feature map is:

$$\mathbf{V}_{\mathrm{vfc\_MGRL}}(x,y) = f_{\mathrm{MGRL}}(x,y) \times \mathbf{k}(x,y) \tag{2}$$

where $\mathbf{k}(x, y)$ is the vector field kernel, the details of which could be referred to [32].

The VFC snakes based on the improved external force minimize the following energy function [32].

$$E = \int_0^1 \left[\frac{1}{2}(\alpha|C^{(1)}(s)|^2 + \beta|C^{(2)}(s)|^2) + E_{\mathrm{vfc\_MGRL}}(C(s))\right] ds \tag{3}$$

where $C(s) = [x(s), y(s)]$, $s \in [0, 1]$ denotes the parametric contour which is defined in an image domain and can move under the influence of the internal and external forces. α and β are weighting parameters representing the degrees of elasticity and rigidity of the parametric contour, respectively. $E_{\mathrm{vfc\_MGRL}}$ denotes the improved external energy. Using the calculus of the variations [21], the minimization of Eq. (3) must satisfy the Euler equation:

$$\alpha \cdot C^{(2)}(x,y) - \beta \cdot C^{(4)}(x,y) + V_{\mathrm{vfc\_MGRL}}(x,y) = 0 \tag{4}$$

where $\mathbf{V}_{\mathrm{vfc\_MGRL}}(x, y) = [u(x, y), v(x, y)]$ is defined as Eq. (2). Using a finite difference approach on a discrete grid, the solution of the Eq. (4), $C(s)$, is the desired boundary of the lymphocyte.

Active contour models allow us to solve both segmentation and tracking problems simultaneously. The concept is that lymphocyte tracking is realized by lymphocyte segmentation frame by frame. To alleviate initialization sensitivity problem, the initial contour of the first frame is obtained around the ground truth by an initial segmentation; the initial contour of the subsequent frame is obtained from the previous frame. That is to say, the final contour of the previous frame is regarded as the initial contour of the current frame during the evolution of active contours. The procedure of segmentation and tracking is described in Fig. 1.

The segmentation and tracking results of the lymphocyte in the image sequence are shown in Fig. 2.

2.3. Methods of features extraction

Once the boundary of the target cell has been obtained, the next step is a concise, quantitative and biologically relevant description of the cell morphology and mobility. In this study, we extracted the features of the shape, the shape deformation and the intracellular

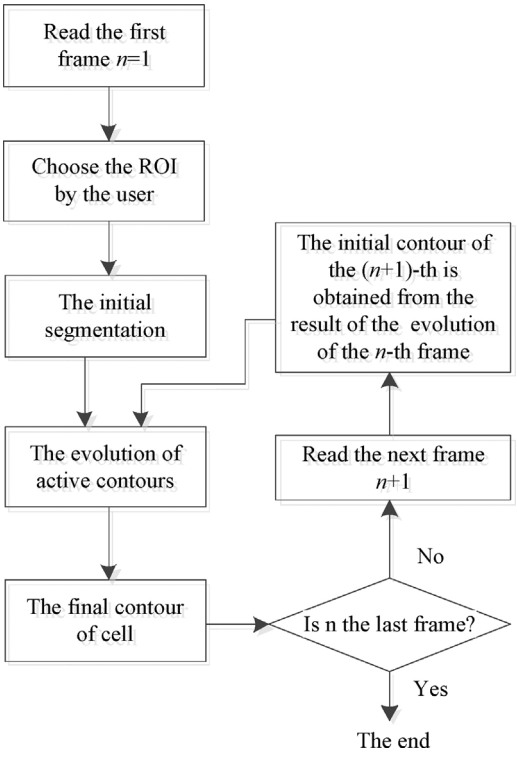

Fig. 1. The workflow of segmentation and tracking of the lymphocyte in an image sequence.

motion, respectively. Methods of features extraction are introduced as follows.

2.3.1. *Shape features extraction* (V_{shape})

In general, shape descriptor is a set of parameters that are produced to describe a given shape. A shape descriptor is consistent with human intuition. Good shape descriptors are supposed to find similar shapes from a database effectively. Some geometric features can be used to describe a shape in different aspects [8,33]. These shape parameters are area, perimeter, center of gravity, eccentricity, circularity, average bending energy, rectangularity, convexity and solidity. Area is the total number of pixels in the region

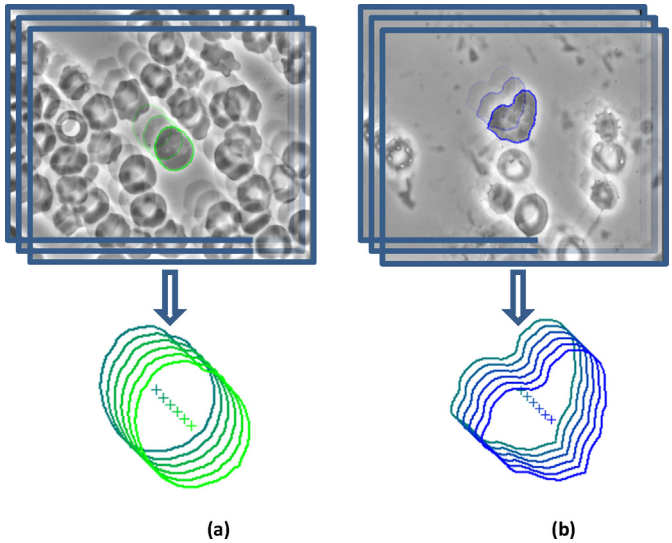

Fig. 2. Cell boundaries tracking. (a) The lymphocyte in the SST group. (b) The lymphocyte in the AST group.

Table 1
Shape description parameters of the object.

Shape parameters	Expressions	Introductions
Circularity	$\mathrm{Cir} = \frac{P^2}{4\pi A}$	P and A are the perimeter and the area of the region containing the object, respectively.
Average bending energy	$\mathrm{ABE} = \frac{1}{N_1}\sum_{k=1}^{N_1} c^2(k)$	$c(k)$ is the curvature of point k; N_1 is the number of points on a boundary.
Rectangularity	$\mathrm{Rect} = \frac{A}{A_R}$	A_R is the area of the minimum bounding rectangle.
Convexity	$\mathrm{Convexity} = \frac{P_{\mathrm{convexhull}}}{P_{\mathrm{shape}}}$	$P_{\mathrm{convexhull}}$ is the perimeter of the convex hull; P_{shape} is the perimeter of the original boundary.
Solidity	$\mathrm{Solidity} = \frac{A}{A_{\mathrm{convexhull}}}$	$A_{\mathrm{convexhull}}$ is the area of the convex hull of the object.

containing the object. Perimeter is the distance around the boundary of the object. Eccentricity is the ratio of the distance between the foci of the ellipse and its major axis length, whose value is between 0 and 1. Circularity ratio represents how a shape resembles a circle. The solidity describes the concavo-convex information of a shape. For example, the solidity of a convex shape is always 1. Some definitions of shape parameters are shown in Table 1.

The shape parameters in Table 1 are defined for the static objects. Here we propose the shape descriptor and the deformation descriptor for describing the shape and the deformation of the lymphocyte in the image sequence as follows. We define the shape descriptor V_{shape} to describe the shape feature of the lymphocyte in the image sequence, as is shown in Eq. (5).

$$V_{\mathrm{shape}} = \frac{1}{N}\sum_{i=1}^{N} D_i \tag{5}$$

where N is the total number of frames in the image sequence; D_i is the shape descriptor value of the lymphocyte in the ith frame, which can be a shape parameter as mentioned above, such as area, perimeter, eccentricity, circularity, average bending energy, rectangularity, convexity and solidity. For example, when D_i represents the area, we get the V_{shape} of area. V_{shape} is the average of the cell shape parameter of all frames in the image sequence, which indicates the shape feature of the lymphocyte in the image sequence.

2.3.2. *Deformation features extraction* ($V_{deformation}$)

We define the deformation descriptor $V_{\mathrm{deformation}}$ to describe the shape change feature of the lymphocyte in the image sequence, which is shown as:

$$V_{\mathrm{deformation}} = \frac{1}{N-1}\sum_{i=2}^{N} |D_i - D_{i-1}| \tag{6}$$

where N and D_i are the same as in Eq. (5); $V_{\mathrm{deformation}}$ is the average of the cell shape difference of all frames in the image sequence, which indicates the deformation feature of the lymphocyte in the image sequence. $V_{\mathrm{deformation}}$ of the area and the perimeter should be normalized.

2.3.3. *Intracellular motion feature extraction based on optical flow*

According to the clinical observation, the intracellular movement is intense in the abnormal group, while slight in the normal group. Here we adopt optical flow techniques to obtain quantitative analysis of intracellular movement. The optical flow computation is a key technique for the object motion analysis, and can help us

to know important motion characteristics of moving bodies. In our study, the camera and the microscopic slide are fixed during the image sequence acquisition process. We assume that the incident illumination is uniform.

Phase contrast microscope is one of the most common used instruments to observe long-term cell activity [34]. Cells are transparent objects and have local variation, and the local phase variations will be generated based on the refractive index while light going through them. Then phase contrast microscopy can generate high-contrast images of cells by translating these local phase variations of the object into intensity variations in the image. So we can apply optical flow method to obtain the velocities of the intracellular motion.

2.3.3.1. Optical flow. The optical flow constraints equation based on BCM is shown as follows [29]:

$$I_x \cdot u + I_y \cdot v + I_t = 0 \tag{7}$$

where $I(x, y, t)$ denotes the image brightness at the point (x, y) in the image at time t. I_x, I_y and I_t are the partial derivatives of image brightness with respect to x, y and t, respectively. $u = dx/dt$ and $v = dy/dt$ are x and y components of the optical flow.

There is only one constraint at each pixel, while a velocity vector has two unknowns: u and v. So the velocity vector cannot be computed locally in Eq. (7), and additional constraint should be involved. Some references have assumptions on the instantaneous velocity field, such as spatial smoothness constraint or spatial constancy in a small neighborhood in the velocity vector [29,35]. Here we use HS optical flow method, in which the additional constraint is to minimize the sum of the square of the magnitude of the gradient of the optical flow. The variation formulation of the HS optical flow method can be expressed as:

$$E_{\mathrm{HS}}(u, v) = \int\int_{\Omega} (I_x \cdot u + I_y \cdot v + I_t)^2 + \gamma(|\nabla u|^2 + |\nabla v|^2)\, dx\, dy \tag{8}$$

where γ is the weighting parameter that controls the relative importance of the optical flow error $(I_x u + I_y v + I_t)$ and the spatial smoothness error $(|\nabla u|^2 + |\nabla v|^2)$. We minimize the sum of the optical flow error and the spatial smoothness error by using the calculus of variations. Hence the optical flow (u, v) that minimize Eq. (8) must satisfy the Euler equation

$$\begin{cases} (I_x \cdot u + I_y \cdot v + I_t)I_x - \gamma \cdot \nabla^2 u = 0 \\ (I_x \cdot u + I_y \cdot v + I_t)I_y - \gamma \cdot \nabla^2 v = 0 \end{cases} \tag{9}$$

The details of the solution process of (u, v) can be found in [29]. Then we can obtain the direction and magnitude of each pixel's velocity of intracellular motion at the cellular stage.

2.3.3.2. Intracellular motion feature (V_{motion}). In order to assess the intracellular motion, we extracted the quantitative feature from the optical flow fields by the following steps. First, we computed the mean velocity of each optical flow field as follows:

$$V_{\mathrm{MeanVeloField}} = \frac{1}{A_\Omega} \sum_{(x,y)\in\Omega} \sqrt{u^2(x, y) + v^2(x, y)} \tag{10}$$

where $u(x, y)$ and $v(x, y)$ are the x and y components of the velocity at the point (x, y). A_Ω is the area of the region Ω. Ω is a closed 2-dimensional optical flow field domain

$$\Omega = \{(x, y) : \sqrt{u^2(x, y) + v^2(x, y)} \geq \text{thresholds}\} \tag{11}$$

where thresholds = 0.0001 (fixed by numerous experiments), which is used to restrict the region of the optical flow fields and mask the optical flow data to the interior of the cell. Secondly, we defined V_{motion} as the intracellular motion feature, which is computed as:

$$V_{\mathrm{motion}} = \frac{1}{N_2} \sum_{i=1}^{N_2} V_{\mathrm{MeanVeloField}\_i} \tag{12}$$

where $V_{\mathrm{MeanVeloField}\_i}$ is the mean velocity of the ith frame optical flow field. N_2 is the total number of frames of the optical flow fields in the image sequence. V_{motion} represents the mean velocity of intracellular movement fields of all frames in an image sequence.

2.4. Two comparative methods

In order to evaluate the performance of our proposed scheme, we also adopt the other two comparative methods in this study: the Fourier descriptor and the Zernike moments. Fourier descriptors (FD) have been successfully applied to contour-based shape representation application, which is appropriate to a close contour shape descriptor [36,37]. Generally, FD is obtained through Fourier transform (FT) on a shape signature function, which is derived from the shape boundary coordinates $\{(x_0, y_0), (x_1, y_1), \ldots, (x_{N-1}, y_{N-1})\}$. Here the complex number derived from the contour $c(n) = x_n + j \cdot y_n$ is used as the shape signature function. One-dimensional FT is then applied on $c(n)$ to obtain the Fourier transformed coefficients.

$$d(k) = \frac{1}{N_3} \sum_{n=0}^{N_3-1} c(n) \exp(-j2\pi nk/N_3), \quad k = 0, 1, \ldots, N_3 - 1 \tag{13}$$

where N_3 is the number of pixels on the cell boundary, and j is the imaginary unit. The coefficients $d(k)$ are used to obtain FD. $d(0)$ denotes the position information of the object shape, and getting rid of it can realize that FD is invariant to translation. Then the magnitudes of the rest of the coefficients normalized by the magnitude of the primary harmonic coefficient $d(1)$ are used as FD. The obtained FD is translation, rotation and scale invariant [37].

Zernike moments descriptor (ZMD) is a region-based shape representation method, which is obtained by using all the pixel information within a shape region. The complex Zernike moments of order n with repetition m are defined as:

$$A_{nm} = \frac{n+1}{\pi} \sum_x \sum_y f(x, y) V^*_{nm}(x, y) \tag{14}$$

where $f(x, y)$ is a binary shape function; n and m are integers, and $V^*_{nm}(x, y)$ is the complex conjugate of $V_{nm}(x, y)$. $V_{nm}(x, y)$ is the Zernike polynomials which are a complete set of complex function orthogonal over the unit disk. The details of $V_{nm}(x, y)$ are referred to [38].

3. Experiments and results

3.1. Experiments

A total of 40 cell image sequences from the recordings were used in our study (20 from each of the two groups). Each image sequence lasts for 20–30 s and the frame rate is 25 frames per second (every image sequence includes 500–750 frames). The first 500 frames of each image sequence were sampled uniformly (selecting every tenth frame) to obtain a 50-frame clip. There is only one-object-lymphocyte in the center of the view in each image sequence. The improved VFC snakes were used to segment and track the cell boundaries in the clip. The whole experiment included two parts: first, shape, deformation and intracellular features were extracted and an optimal feature vector was chosen by statistical analysis. The shape feature V_{shape}, the deformation feature $V_{\mathrm{deformation}}$ and the motion feature V_{motion} will be combined to characterize the

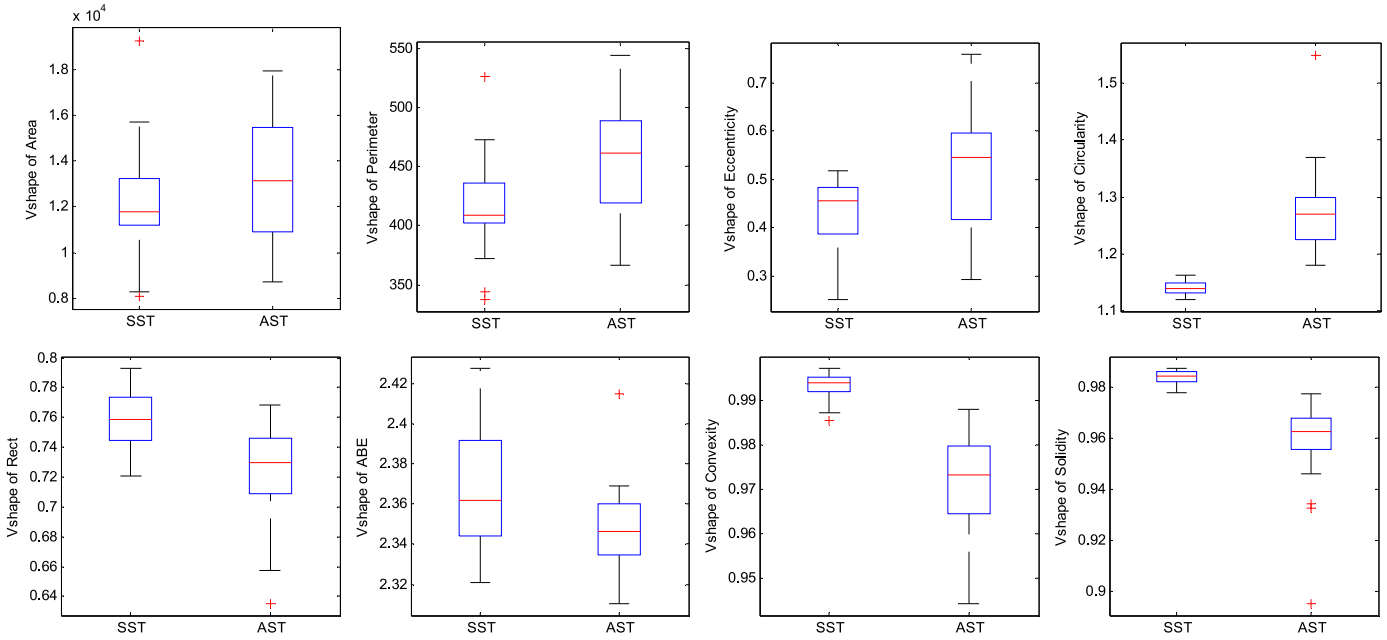

Fig. 3. Boxplot of the extracted shape descriptors. The vertical axis is the V_{shape} values of area, perimeter, eccentricity, circularity, average bending energy, rectangularity, convexity and solidity, respectively.

cell dynamic behavior in the experiments. Second, PNN was used to evaluate the performance of our scheme.

3.2. Results of features extraction

For each 50-frame clip, the shape features (area, perimeter, eccentricity, circularity, average bending energy, rectangularity, convexity and solidity) of the lymphocyte in each frame were computed. Subsequently, V_{shape} and $V_{\text{deformation}}$ of each clip were computed according to Eqs. (5) and (6), respectively. The V_{shape} and $V_{\text{deformation}}$ values of the object-cell from 40 image sequences were shown in box whisker plots Figs. 3 and 4, respectively. In these plots, the left and right box respectively denotes the results from the SST and AST group.

The results of the intracellular motion are presented as follows. In each 50-frame clip, pairs of frames taken at an interval of 4 (frame 1 and 5, 2 and 6, . . .) were used to compute a frame of optical flow field. Then 46 different optical flow fields were obtained from each 50-frame clip. The optical flow fields are representative of the intracellular motion fields, in which each vector show the direction and magnitude of each pixel's velocity, as is shown in Fig. 5(c). In order to display the intracellular motion vividly, the optical flow field is sampled every 5×5 pixels, and is magnified 5 times in Fig. 5(c). The direction of the arrow in the optical flow field denotes the direction

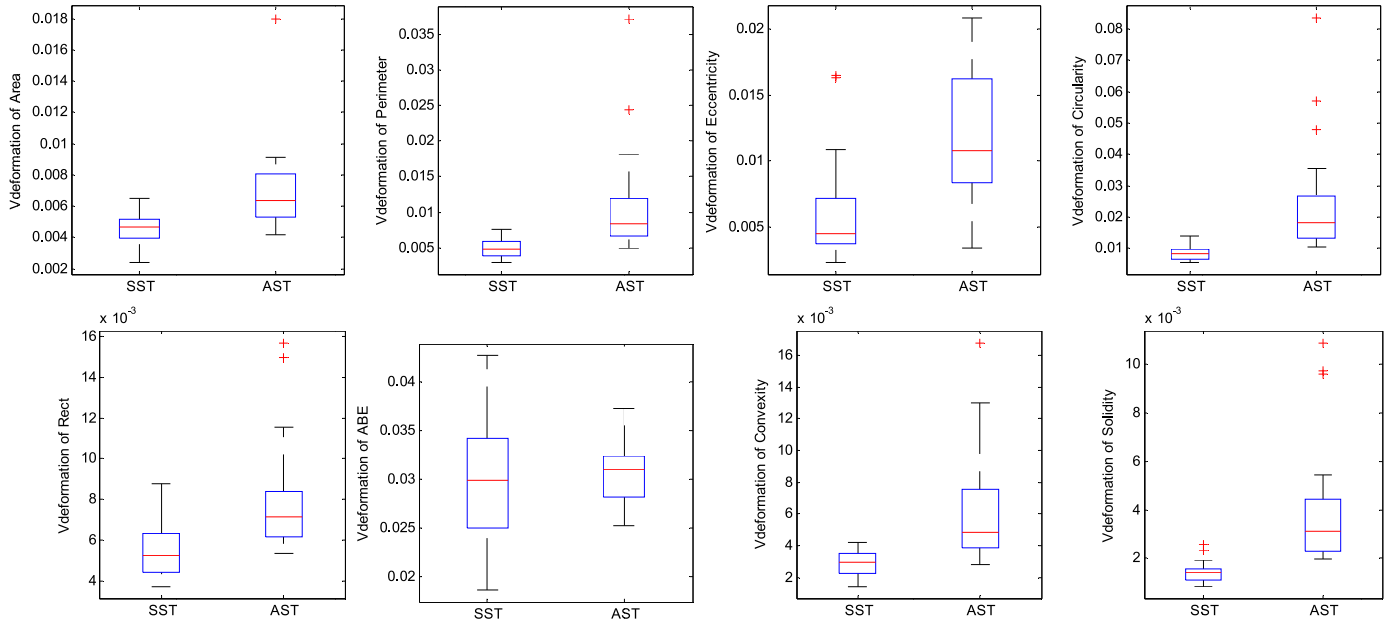

Fig. 4. Boxplot of the extracted deformation descriptors. The vertical axis is the $V_{\text{deformation}}$ values of area, perimeter, eccentricity, circularity, average bending energy, rectangularity, convexity and solidity, respectively.

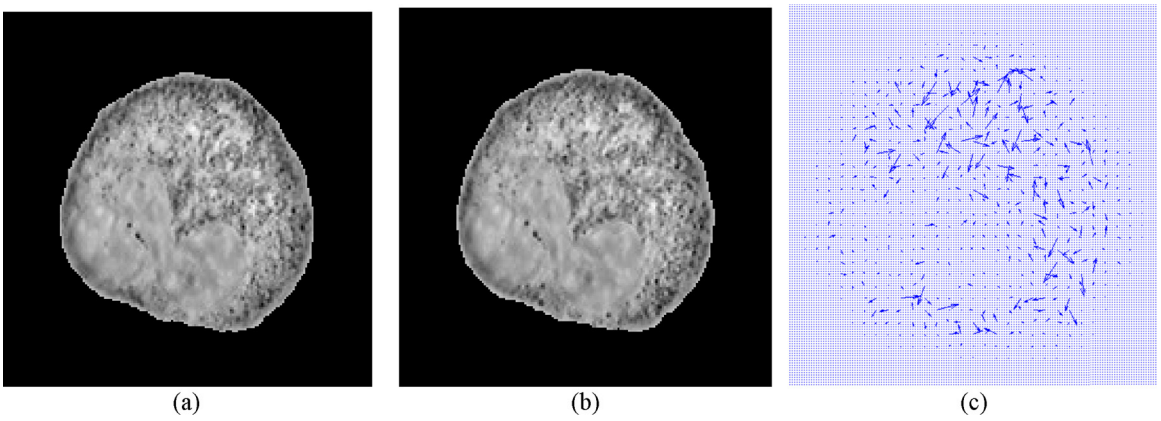

Fig. 5. (a) The nth frame. (b) The $(n+4)$th frame. (c) The optical flow field of the intracellular motion based on (a) and (b).

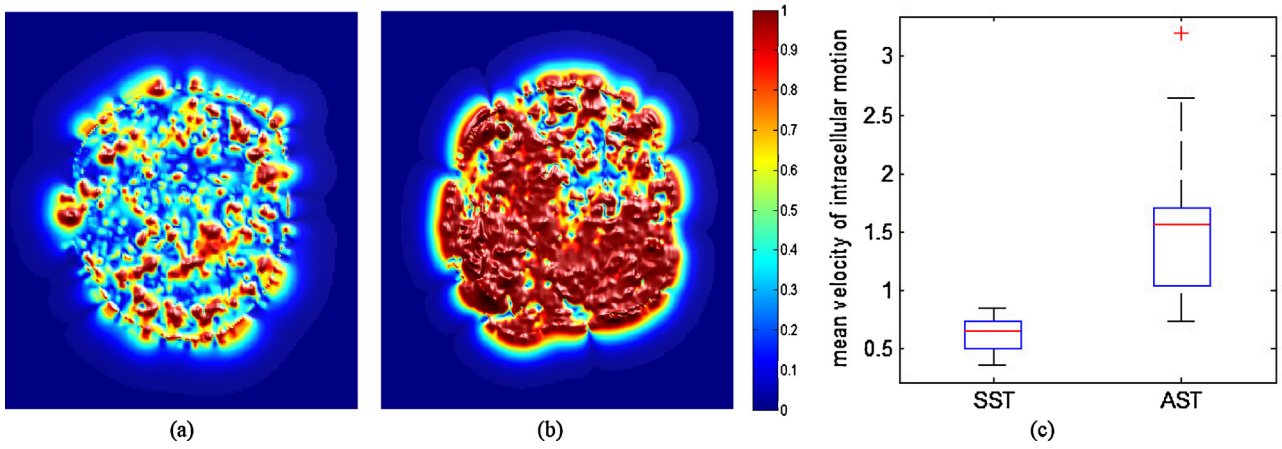

Fig. 6. Examples of Intracellular motion by color coding from (a) the normal lymphocyte; (b) the abnormal lymphocyte. Red represents fast velocity, while blue represents slow velocity. (c) Boxplot of the extracted intracellular motion feature. The vertical axis denotes the V_{motion} value of the images sequences. (For interpretation of the references to color in this figure legend, the reader is referred to the web version of this article.)

of the intracellular motion, and the length of the arrow denotes the magnitude of the intracellular motion.

In addition, we randomly selected two videos, with one from the SST and the other from the AST group, computed the optical flow field of the intracellular motion, and then extracted the magnitude of the optical flow, as is shown by color coding in Fig. 6(a) and (b). Finally, we calculated the intracellular feature V_{motion} of 40 cell image sequences according to Eq. (12), with the experimental result given in box whisker plot Fig. 6(c).

3.3. Comparative experiments

The FD method, known as a conventional boundary-based shape descriptor method, and the ZMD, as a classical region-based method, are adopted in the article for the comparative experiments. The processes of these two extraction features are as follows: first, for each image of the 50-frame clip, the FD and ZMD (order = 20) features are computed respectively. Then the similarity between successive images is measured by the Euclidean distance of shape feature descriptors of images. Then the mean value of shape features descriptors variations is calculated as the deformation features of the clip. The results are shown in box whisker plot Fig. 7.

3.4. Statistical analysis

In order to choose optimal features as the feature vector to characterize the dynamic behavior of the lymphocytes, we apply Wilcoxon rank sum test to identify the extracted features that have the best power in distinguishing the two groups. All the V_{shape} parameters and the corresponding $V_{\text{deformation}}$ parameters are included in the rank sum test. The results of these tests indicate that the differences with respect to the V_{shape} values between the two groups are statistically significant for circularity, convexity and solidity ($p < 0.0001$). With respect to the $V_{\text{deformation}}$ features, the statistic results show that more features have significant differences. These features include $V_{\text{deformation}}$ of area, perimeter, circularity, convexity and solidity, which are chosen based on the p-values < 0.0001. The features with the smallest p-values of V_{shape} and $V_{\text{deformation}}$ are chosen as the optimal features in this study. Then for V_{motion}, the corresponding result of the

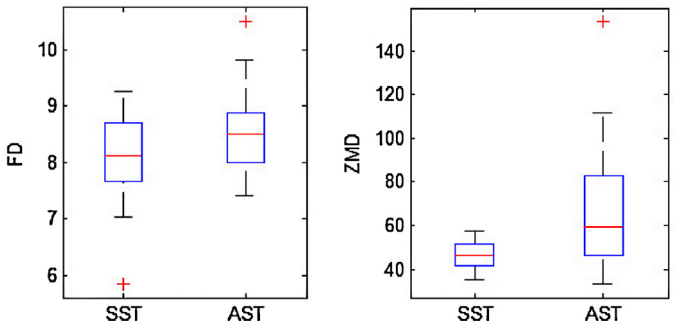

Fig. 7. Boxplot of the extracted features based on FD and ZMD methods.

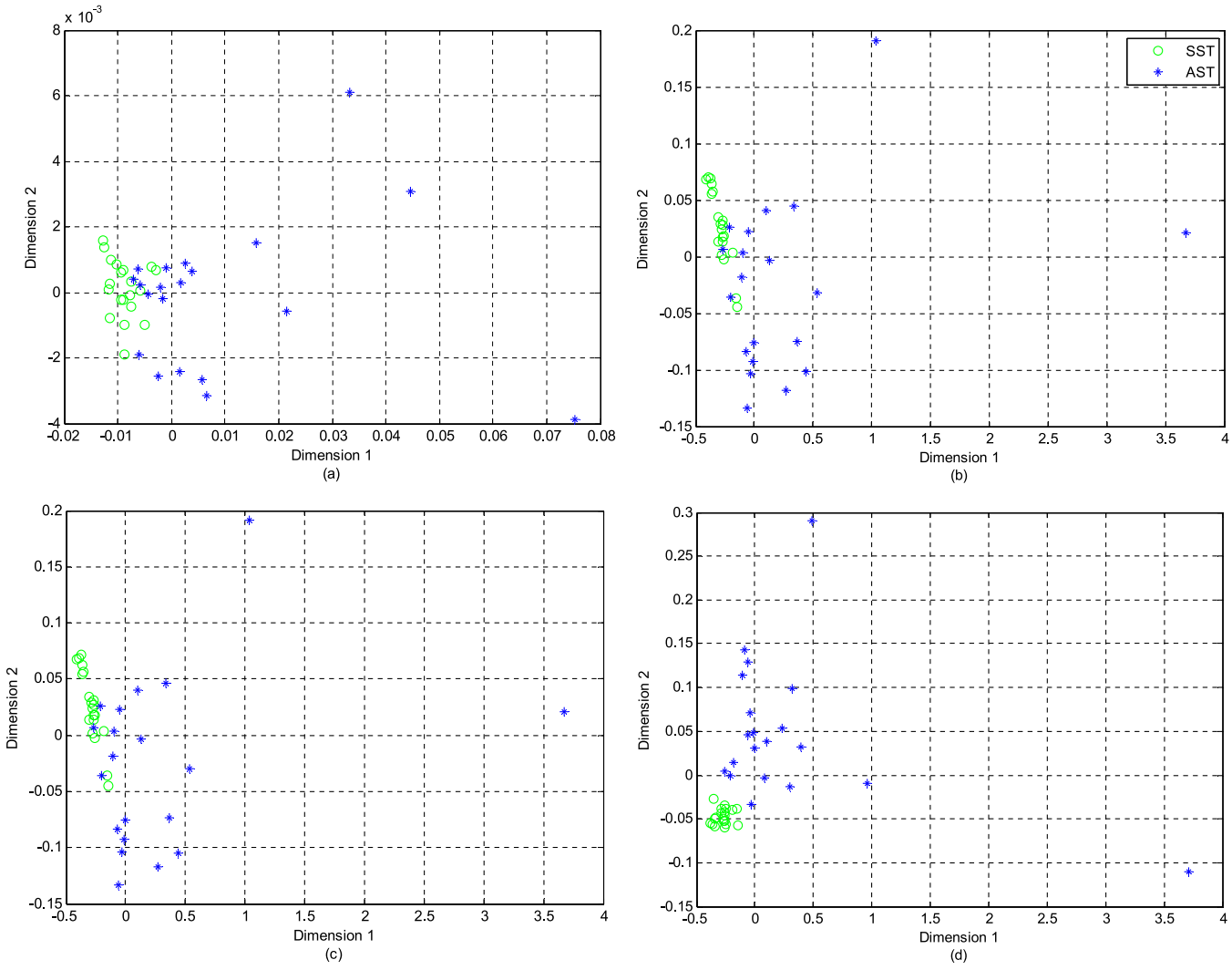

Fig. 8. MDS projections of feature vector distances between 40 image sequences (20 from each of the two groups); the circle denotes the SST group and the star denotes the AST group. (a) Only use the shape descriptors. (b) Only use the deformation descriptors. (c) Only use the motion descriptors. (d) Combine the features of the shape, the deformation and the intracellular motion.

test is $p = 1.6571e{-}05$. With respect to FD, $p = 0.0810$; the case of ZMD is $p = 0.0090$. The results indicate that the FD technique, as a boundary-based shape descriptor, fails to describe the characteristics of the cell dynamic behavior in this study, while ZMD technique, which is based on region information, could be used to express the cell dynamic behavior of the two groups.

3.5. Classification results

According to the findings from the Wilcoxon rank sum tests, the features which possess the smallest p-values between the two test groups are combined as a feature vector of the lymphocyte dynamic behavior. The feature vector is defined as the combination of the shape descriptors V_{shape} values in terms of circularity, convexity and solidity, the deformation descriptors $V_{\text{deformation}}$ values in terms of area, perimeter, circularity, convexity and solidity, and V_{motion} (intracellular motion). That is to say, the activity of the lymphocyte in each image sequence is represented by a 9-parameter feature vector. In order to compare the effect of different combined features to classify the two kinds of data, the distances of different combined features in 40 image sequences were visualized by projecting the feature vector matrix onto a two-dimensional plane using multidimensional scaling (MDS), as shown in Fig. 8.

PNN is used to classify the two categories of image sequences. We compared the results of the joint features with several other schemes such as using shape features (S-Features) only, using deformation features (D-Features) only, using intracellular motion feature (M-Features) only, using shape and deformation features (S&D-Features), using shape and intracellular motion features (S&M-Features), and using deformation and intracellular motion features (D&M-Features). The feature derived from the ZMD method is also used in the classification experiments. The contrast experiment schemes and the corresponding classification rates are shown in Table 2, in which S&D&M-Features indicate using

Table 2
Classification results of cell image sequences by using PNN.

Features	Sen (%)	Spe (%)	FaP (%)	FaN (%)	Rer (%)
Motion (M)	88.39	91.87	8.44	11.21	90.13
Deformation (D)	89.88	90.15	9.87	10.07	90.03
Shape (S)	86.26	85.88	14.05	13.80	86.08
S&D	91.67	94.70	5.47	8.10	93.18
S&M	90.14	91.25	8.85	9.74	90.70
D&M	92.34	93.52	6.58	7.56	92.93
ZMD	86.51	84.03	15.61	13.84	85.26
S&D&M	94.82	97.83	2.22	5.05	96.33

the combination of shape, deformation and intracellular motion features, which is a 9-parameter feature vector as input to PNN. Sensitivity (Sen) means the probability that the test says an image sequence is from the AST group while in fact it is from the AST group. Specificity (Spe) is defined as the probability that the test says an image sequence is from the SST group while in fact it is from the SST group. A false positive (FaP) occurs when the test reports an AST result while in fact for an image sequence which is from the SST group. A false negative (FaN) occurs when the test reports an SST result while in fact for an image sequence which is from the AST group. Rer denotes the recognition rate.

4. Discussion

In this article, we proposed a novel scheme for characterizing the dynamic behavior of lymphocytes in microscopic images. We modeled the relationships between the immune status of the organism and the activity of the immune cells (lymphocytes) through analyzing the dynamic behavior of the lymphocytes. Then we studied the dynamic behavior of the lymphocytes in three aspects: the shape, the deformation and the intracellular motion.

As the results shown in Fig. 3 as well as in the statistical tests, the shape descriptor V_{shape} with respect to circularity, convexity and solidity have statistically significant differences between the normal and the rejection groups. In addition, the deformation descriptors, $V_{\text{deformation}}$ values in terms of area, perimeter, circularity, convexity and solidity, can be used to differentiate the normal and rejection cases, as shown in Fig. 4 and the results of the statistical tests. This also indicates that the deformation descriptors are more sensitive in describing the difference of the lymphocyte behavior between the two data groups. Fig. 6(c) shows that the velocity of intracellular movement in the AST group is greater than that in the SST group, and the statistical result shows that the intracellular motion feature has a significant difference between the two data groups. Given the results from these statistical tests, a set of optimal features are chosen to form a feature vector for neural network based classification.

Comparative experimental results, as shown in Fig. 7 and in the statistical results, indicate that the features based on the FD have no statistically significant differences between the two groups of data, presumably attributable to the use of boundary-based shape descriptor therein, which has the drawback of losing region information. Therefore it virtually adds no value to the subsequent classification test if used. Meanwhile, according to the statistical result, the ZMD feature is effective in our study, which certainly arises from the use of region information in this feature.

We also project the distances of the different combination feature vector matrix of the 40 data onto a two-dimensional plane using MDS, as shown in Fig. 8. And the result indicates that the combined features yield the best performance, which is consistent with the statistical result. To further evaluate the quality of the optical feature vector, PNN is used to classify the lymphocyte dynamic behavior. Of particular notes, according to the recognition rate in Table 2, the contribution of the intracellular motion features is relatively large, as well as that of the deformation features, whereas the shape features have the smallest contribution to the diagnosis of graft rejection. The performance of ZMD is a little lower than the S-Features because it exploits the region information of the live cell, but it comes at the cost of much higher computational complexity. The results of Table 2 also show that the feature vector, which takes advantages of the three aspects (shape, deformation and intracellular motion) of the lymphocyte dynamic behavior, achieves the highest recognition rate. The result agrees well with the clinical pathological phenomena that graft rejection increases intracellular motion, and causes cell boundaries to change dramatically, i.e. cell deformation and protrusion. Thus, our proposed scheme is suitable for describing and analyzing this dynamic behavior of cells, which is clearly supported by the best recognition rate shown in Table 2.

As briefly mentioned above, according the experimental results, the features that simultaneously exploit the shape, shape deformation and intracellular motion information exhibit best performance in characterizing the differences between the normal and abnormal data, which well conforms with clinicians' observation: the activity of lymphocytes is enhanced during graft reaction, i.e., the lymphocytes in the abnormal group have dramatic deformation, while the lymphocytes in the normal group are more stable. Thus, based on the findings from this work, it is evident that the proposed scheme could be used to better understand the immune status of the organism and to predict graft rejection based on quantitative and qualitative assessment of the lymphocyte dynamic behavior in the peripheral blood. This offers the potential of developing a minimum-invasive and more convenient method to predict and detect the graft rejection, as compared with conventional biopsy, since acquiring the peripheral blood is less invasive and more convenient than the biopsy.

Finally, it should be pointed out that this study also has its own limitations. First, our effort was motivated by clinicians' observation that the lymphocytes in the human peripheral blood have more morphological changes when the patient, who receives the liver transplant, gets the graft rejection. Once the graft rejection occurs, the doctor should give appropriate amount of medicine to restrain the graft rejection. Since the immune status of the human being is hard to control, the doctor usually gives medicine to restrain the graft rejection prior to its occurrence, otherwise the patient is in danger. For these reasons, our experiment used mice instead of human beings, and skin transplant rather than liver transplant. Second, T cells (a kind of lymphocytes) are the major cellular components of the adaptive immune response, and T cells are involved in cell-mediated immunity. Here based on the clinicians' long term observation, T cells are more active when the graft rejection occurs, which has provided the rationale for the use of lymphocytes as the research target in this study. The morphology and dynamic of other cells may also have predictive values for graft rejection, the study of which is however beyond the scope of this work but is envisioned as our focus in the future. In addition, there is obvious particle motion intra-lymphocyte, and thus we have focused on quantitative analysis of the intracellular motion. While the methods introduced in [5,25] treat the cell as a whole to analyze cell motion, but they are unable to express the intracellular motion information clearly. For this reason, we did not compare our intracellular motion results with the method mentioned in [5,25].

5. Conclusion

In this article we have proposed a scheme for quantitatively analyzing the shape, deformation, and intracellular motion of lymphocyte in microscopic image sequences, and applied it to the study of the dynamic behavior of lymphocyte in the peripheral blood of mice post skin transplantation. The contributions of the proposed method are two-fold: first, we have presented a novel approach for quantitative analysis of intracellular motion based on optical flow techniques, which can compute the intracellular motion field and show the direction and magnitude of intracellular motion at every pixel location. Second, we have presented a comprehensive quantitative analysis of cell dynamic behavior by combining features of the cell shape, deformation, and intracellular motion. The Wilcoxon rank sum test was used to choose the best features to form an optimal feature vector. PNN is used to classify lymphocytes dynamic behavior based on the feature vector. Experimental results show that the proposed scheme for characterizing the dynamic behavior of the lymphocyte achieve a better performance than the FD or ZMD methods because of its advantages in combing the shape,

deformation and intracellular motion features of the live lymphocyte, leading to its potential applications to improved diagnostic and interventional strategies for the graft rejection.

Conflicts of interest

The authors report no declarations of interest.

Acknowledgments

This work was supported by the National Natural Science Foundation of China (61271112). The authors would like to thank the president of Beijing You'an Hospital, Ning Li, for providing the microscopic cell image sequences.

References

[1] E. Meijering, O. Dzyubachyk, I. Smal, W.A. van Cappellen, Tracking in cell and developmental biology, Semin. Cell Dev. Biol. 20 (2009) 894–902.
[2] R. Ananthakrishnan, A. Ehrlicher, The forces behind cell movement, Int. J. Biol. Sci. 3 (2007) 303–317.
[3] F. Biname, G. Pawlak, P. Roux, U. Hibner, What makes cells move: requirements and obstacles for spontaneous cell motility, Mol. Biosyst. 6 (2010) 648–661.
[4] N. Ray, S.T. Acton, K. Ley, Tracking leukocytes in vivo with shape and size constrained active contours, IEEE Trans. Med. Imaging 21 (2002) 1222–1235.
[5] F. Germain, A. Doisy, X. Ronot, P. Tracqui, Characterization of cell deformation and migration using a parametric estimation of image motion, IEEE Trans. Biomed. Eng. 46 (1999) 584–600.
[6] C. Zimmer, E. Labruyere, V. Meas-Yedid, N. Guillen, J.C. Olivo-Marin, Segmentation and tracking of migrating cells in videomicroscopy with parametric active contours: a tool for cell-based drug testing, IEEE Trans. Med. Imaging 21 (2002) 1212–1221.
[7] N.H. Nguyen, S. Keller, E. Norris, T.T. Huynh, M.G. Clemens, M.C. Shin, Tracking colliding cells in vivo microscopy, IEEE Trans. Biomed. Eng. 58 (2011) 2391–2400.
[8] Z. Pincus, J.A. Theriot, Comparison of quantitative methods for cell-shape analysis, J. Microsc. 227 (2007) 140–156.
[9] J.R. Swedlow, K.W. Eliceiri, Open source bioimage informatics for cell biology, Trends Cell Biol. 19 (2009) 656–660.
[10] J.R. Swedlow, Advanced hardware and software tools for fast multidimensional imaging of living cells, Proc. Natl. Acad. Sci. U. S. A. 107 (2010) 16005–16006.
[11] T. Tolxdorff, T.M. Deserno, H. Handels, H.P. Meinzer, Advances in medical image computing, Methods Inf. Med. 48 (2009) 311–313.
[12] Y. Xiong, P.A. Iglesias, Tools for analyzing cell shape changes during chemotaxis, Integr. Biol. 2 (2010) 561–567.
[13] C. Terryn, A. Bonnomet, J. Cutrona, C. Coraux, J.M. Tournier, B. Nawrocki-Raby, M. Polette, P. Birembaut, J.M. Zahm, Video-microscopic imaging of cell spatio-temporal dispersion and migration, Crit. Rev. Oncol. Hematol. 69 (2009) 144–152.
[14] K. Solez, History of the Banff classification of allograft pathology as it approaches its 20th year, Curr. Opin. Organ Transplant. 15 (2010) 49–51.
[15] I.T. Young, The classification of white blood cells, IEEE Trans. Biomed. Eng. 19 (1972) 291–298.
[16] F.P. Ferrie, M.D. Levine, S.W. Zucker, Cell tracking: a modeling and minimization approach, IEEE Trans. Pattern Anal. Mach. Intell. 4 (1982) 277–291.
[17] D.P. Mukherjee, N. Ray, S.T. Acton, Level set analysis for leukocyte detection and tracking, IEEE Trans. Image Process. 13 (2004) 562–572.
[18] O. Debeir, P. Van Ham, R. Kiss, C. Decaestecker, Tracking of migrating cells under phase-contrast video microscopy with combined mean-shift processes, IEEE Trans. Med. Imaging 24 (2005) 697–711.
[19] A.J. Hand, T. Sun, D.C. Barber, D.R. Hose, S. MacNeil, Automated tracking of migrating cells in phase-contrast video microscopy sequences using image registration, J. Microsc. 234 (2009) 62–79.
[20] Y.N. Sun, C.H. Lin, C.C. Kuo, C.L. Ho, C.J. Lin, Live cell tracking based on cellular state recognition from microscopic images, J. Microsc. 235 (2009) 94–105.
[21] G. Apostolopoulos, S.V. Tsinopoulos, E. Dermatas, A methodology for estimating the shape of biconcave red blood cells using multicolor scattering images, Biomed. Signal Process. Control 8 (2013) 263–272.
[22] G. Thurston, B. Jaggi, B. Palcic, Measurement of cell motility and morphology with an automated microscope system, Cytometry 9 (1988) 411–417.
[23] F. Siegert, C.J. Weijer, A. Nomura, H. Miike, A gradient method for the quantitative analysis of cell movement and tissue flow and its application to the analysis of multicellular dictyostelium development, J. Cell Sci. 107 (1994) 97–104.
[24] Y. Sato, J. Chen, R.A. Zoroofi, N. Harada, S. Tamura, T. Shiga, Automatic extraction and measurement of leukocyte motion in microvessels using spatiotemporal image analysis, IEEE Trans. Biomed. Eng. 44 (1997) 225–236.
[25] X. Ronot, A. Doisy, P. Tracqui, Quantitative study of dynamic behavior of cell monolayers during in vitro wound healing by optical flow analysis, Cytometry 41 (2000) 19–30.
[26] K. Keren, Z. Pincus, G.M. Allen, E.L. Barnhart, G. Marriott, A. Mogilner, J.A. Theriot, Mechanism of shape determination in motile cells, Nature 453 (2008) 475–480.
[27] M.K. Driscoll, J.T. Fourkas, W. Losert, Local and global measures of shape dynamics, Phys. Biol. 8 (2011) 055001–055009.
[28] X. An, Z. Liu, Y. Shi, N. Li, Y. Wang, S. Joshi, Modeling dynamic cellular morphology in images, in: N. Ayache, H. Delingette, P. Golland, K. Mori (Eds.), Proceedings of the 15th International Conference on Medical Image Computing and Computer Assisted Intervention, Springer Berlin Heidelberg, Nice, France, 2012, October, pp. 340–347.
[29] B.K.P. Horn, B.G. Schunck, Determining optical flow, Artif. Intell. 17 (1981) 185–203.
[30] Y. Huang, Z. Liu, Y. Shi, N. Li, X. An, X. Gou, Quantitative analysis of lymphocytes morphology and motion in intravital microscopic images, in: The 35th Annual International Conference of the IEEE Engineering in Medicine and Biology Society, IEEE, Oska, Japan, 2013, pp. 3686–3689.
[31] L. Vincent, Morphological grayscale reconstruction in image analysis: applications and efficient algorithms, IEEE Trans. Image Process. 2 (1993) 176–201.
[32] B. Li, S.T. Acton, Active contour external force using vector field convolution for image segmentation, IEEE Trans. Image Process. 16 (2007) 2096–2106.
[33] M. Yang, K. Kpalma, J. Ronsin, A survey of shape feature extraction techniques, Pattern Recognit. (2008) 43–90.
[34] P.J. Davis, E.A. Kosmacek, Y. Sun, F. Ianzini, M.A. Mackey, The large-scale digital cell analysis system: an open system for nonperturbing live cell imaging, J. Microsc. 228 (2007) 296–308.
[35] J.K. Kearney, W.B. Thompson, D.L. Boley, Optical flow estimation: an error analysis of gradient-based methods with local optimization, IEEE Trans. Pattern Anal. Mach. Intell. 9 (1987) 229–244.
[36] R. Chellappa, R. Bagdazian, Fourier coding of image boundaries, IEEE Trans. Pattern Anal. Mach. Intell. 6 (1984) 102–105.
[37] D. Zhang, G. Lu, Study and evaluation of different Fourier methods for image retrieval, Image Vis. Comput. 23 (2005) 33–49.
[38] A. Khotanzad, H. Yaw Hua, Invariant image recognition by Zernike moments, IEEE Trans. Pattern Anal. Mach. Intell. 12 (1990) 489–497.